NANO · MICRO small

www.small-journal.com

High Capacity, Dendrite-Free Growth, and Minimum Volume Change Na Metal Anode

*Yang Zhao, Xiaofei Yang, Liang-Yin Kuo, Payam Kaghazchi, Qian Sun, Jianneng Liang, Biqiong Wang, Andrew Lushington, Ruying Li, Huamin Zhang, and Xueliang Sun**

Na metal anode attracts increasing attention as a promising candidate for Na metal batteries (NMBs) due to the high specific capacity and low potential. However, similar to issues faced with the use of Li metal anode, crucial problems for metallic Na anode remain, including serious moss-like and dendritic Na growth, unstable solid electrolyte interphase formation, and large infinite volume changes. Here, the rational design of carbon paper (CP) with N-doped carbon nanotubes (NCNTs) as a 3D host to obtain Na@CP-NCNTs composites electrodes for NMBs is demonstrated. In this design, 3D carbon paper plays a role as a skeleton for Na metal anode while vertical N-doped carbon nanotubes can effectively decrease the contact angle between CP and liquid metal Na, which is termed as being "Na-philic." In addition, the cross-conductive network characteristic of CP and NCNTs can decrease the effective local current density, resulting in uniform Na nucleation. Therefore, the as-prepared Na@CP-NCNT exhibits stable electrochemical plating/stripping performance in symmetrical cells even when using a high capacity of 3 mAh cm^{-2} at high current density. Furthermore, the 3D skeleton structure is observed to be intact following electrochemical cycling with minimum volume change and is dendrite-free in nature.

1. Introduction

Li-ion batteries (LIBs) are the widely popularized energy storage devices for use in portable electronics and electrical vehicle.[1–4] However, low cost and large scale application remains a significant challenge for LIBs due to the limited and uneven distribution of lithium sources.[5,6] As a promising alternative, Na-ion batteries and Na metal batteries (NMBs) have received a great deal of attention due to sodium's wide availability and low cost. Furthermore, Na metal anode is considered as an attractive candidate compared with other anodes for NMBs due to its high theoretical specific capacity of 1166 mAh g^{-1} and lowest electrochemical potential. Meanwhile, both Na–S batteries and Na–O_2 batteries using Na metal as anodes demonstrate a high theoretical specific energy density of 1274 and 1605 Wh kg^{-1}, respectively.[7–13]

Currently, research efforts in the development of NMBs are primarily focused on the design and fabrication of cathode materials, with little emphasis directed toward the development of Na anode electrode materials. However, similar to issues faced with the use of Li metal anode, crucial problems for metallic Na anode remain. Many of these issues are caused by side reactions occurring between Na metal and the organic liquid-based electrolyte.[14–18] Moss-like and dendritic Na is often observed to be deposited during repetitive Na plating/stripping process with an unstable solid electrolyte interphase (SEI) layer forming on the surface of Na metal anodes. Continuous moss-like and dendritic Na growth will lead to two serious problems: (1) internal short circuit of the battery, presenting serious safety concerns; (2) accumulation of "dead Na" as well as consumption of electrolyte, leading to poor Coulombic efficiency.[6,19,20] Furthermore, the host-less nature of using pure Na metal as an anode results in large infinite volume changes to occur during electrochemical plating/stripping process and presents a difficult materials challenge problem.

To date, there are only few reports exploring the electrochemical plating/stripping properties of Na metal at room temperature. Cui and co-workers first reported the in situ formation of a stable SEI layer by altering components of the electrolyte. Their study demonstrates that mono-, di-, and tetraglyme sodium hexafluorophosphate can enable the reversible and

Y. Zhao, X. Yang, Dr. Q. Sun, J. Liang, Dr. B. Wang, A. Lushington, R. Li, Prof. X. Sun
Department of Mechanical and Materials Engineering
University of Western Ontario
London, Ontario N6A 5B9, Canada
E-mail: xsun@eng.uwo.ca

X. Yang, Prof. H. Zhang
Division of Energy Storage
Dalian Institute of Chemical Physics
Chinese Academy of Sciences
Zhongshan Road 457, Dalian 116023, China

X. Yang, Prof. H. Zhang
The Department of Chemistry and Chemical Engineering
University of Chinese Academy of Sciences
Beijing 100039, China

L.-Y. Kuo, Prof. P. Kaghazchi
Theoretical Electrochemistry
Physikalische und Theoretische Chemie
Freie Universität Berlin
Takustr. 3, D-14195 Berlin, Germany

Prof. P. Kaghazchi
Forschungszentrum Jülich GmbH
Institute of Energy and Climate Research (IEK-1)
Materials Synthesis and Processing
Wilhelm-Johnen-Straße, 52425 Jülich, Germany

DOI: 10.1002/smll.201703717

nondendritic plating/stripping of sodium metal anode.[21] Another strategy is the use of a coating layer to stabilize SEI formation and suppress unwanted side reactions. Atomic layer deposition (ALD) is a technique that provides excellent coverage with conformal deposition in highly controllable manner and can be conducted at relative low deposition temperatures. These features make ALD an ideal technique for Na anode protection.[22,23] Recently, both our group and Hu et al. have successfully demonstrated the application of ALD Al_2O_3 coating layers for the enhancement of electrochemical stability of Na metal anode and suppressed dendrite growth with prolong cycling life time in carbonate and ether based electrolyte systems, respectively.[20,24] Furthermore, our group first reported the use of inorganic–organic coating (alucone) via molecular layer deposition as a protective layer for metallic Na anode.[25] By protecting Na anode with an alucone layer, dendrite and mossy Na formation was effectively suppressed, resulting in prolonged lifetime of Na metal anode.

These strategies are suitable in solving the issue of unstable SEI formation, thereby reducing Na dendrite growth, however, they do not address the large volume changes due to "the hostless" nature of using metallic Na as an anode. To overcome the volume change of Na, it is expected to design different 3D host to hold Na metal with buffering spaces. Get inspiration from the Li protection field, a novel strategy of "thermal infusion" has been reported to achieve 3D scaffold supported Li electrode with minimum volume change and long life time.[26] It has been studied that the wettability between molten metal with the scaffold structure is a key factor in allowing for metal diffusion into the host material. To modify the surface of substrate into "metal-philic," coating layers or N-doped sites are effective to improve the wettability, resulting in uniform nucleation and deposition of metal on the surface.[27–29] Subsequently, Chen and co-workers and Hu et al. reported two types of Na anodes with 3D structures (Na-reduced graphene oxide and Na-carbonized wood), in which confining Na metal anode in a 3D host can significantly enhance stability.[19,30] Despite this, the research and development for the use of Na metal anode remains in its infancy and achieving highly stable Na metal anode with high capacity, minimum volume change and a dendrite free structure remains elusive. Meanwhile, similar phenomenon with lithiophilic, we name "Na-philic" here has not been explored in the previous study.

Herein, we demonstrate the rational design of a carbon paper (CP) with N-doped carbon nanotubes (NCNTs) as a 3D host to obtain Na@CP-NCNTs composites electrodes for NMBs. In our design, 3D carbon paper plays a role as a skeleton for Na metal anode while vertical N-doped carbon nanotubes can effectively decrease the contact angle between CP and liquid metal Na, which we term as being "Na-philic." In addition, the cross-conductive network characteristic of CP and NCNTs can decrease the effective local current density, resulting in uniform Na nucleation. Therefore, the as-prepared Na@CP-NCNTs exhibit stable electrochemical plating/stripping performance in symmetrical cells even when using a high capacity of 3 mAh cm^{-2}, which is highest in the reported literatures using carbonate-based electrolyte. Furthermore, the 3D skeleton structure is observed to be intact following electrochemical cycling with minimum volume change and dendrite-free in nature.

2. Results and Discussion

To encapsulate Na metal into a 3D conductive scaffold, the "Na-philic" NCNTs were introduced to increase the Na wettability of CP. **Figure 1** shows the schematic diagram of the fabrication procedure of Na@CP-NCNTs composites. To assist with the growth of vertical carbon nanotubes, Al_2O_3 was initially deposited on the surface of CP using ALD. NCNTs were obtained through a one-step spray pyrolysis chemical vapor deposition (SPCVD) method, which has been reported in our previous study.[12] Finally, encapsulation of Na metal into the 3D CP-NCNTs structure was accomplished using a thermal infusion process of melting Na in an Ar-filled glove box. Interestingly, without NCNTs, pristine CP was found to be "Na-phobic" and displayed a large contact angle between the substrate and melted Na (Figure S1a, Supporting Information). Promisingly, after functionalizing the CP with NCNTs, the contact angle between Na and CP-NCNTs was effectively reduced (see in Figure S1b, Supporting Information) and Na was found to instantaneously diffuse into the 3D CP-NCNTs, as shown in Figure S1c–e and Video S1 in the Supporting Information. These results demonstrate that NCNTs possess the ability to change Na wettability properties of CP from "Na-phobic" into "Na-philic."

The morphology of obtained CP-NCNTs composites was investigated via scanning electron microscopy (SEM), as shown in Figure S2 in the Supporting Information. Following the SPCVD process, individual cross-stitched carbon fibers are covered uniformly with vertical NCNTs up to 20 μm in length. Figure S3 (Supporting Information) shows the Raman spectra of pristine carbon paper and fabricated CP-NCNTs. The peak at about 1591 cm^{-1} (G band) is related to the vibration of sp^2 bonded carbon atom in 2D hexagonal lattice and the 1329 cm^{-1} (D band) is related to the defects and disorder in the hexagonal graphitic layers. The I_D/I_G of CP-NCNTs is 0.71 while the value of CP is 0.95, suggesting a greater degree of graphitization of carbon deposit during SPCVD and growth of carbon nanotubes.[31] In addition, X-ray photoelectron spectroscopy (XPS) analysis of the CP-NCNTs shown in Figure S4 (Supporting Information) indicates the N content of the samples to be 4.7% (Table S1). The typical high-resolution XPS spectra of N 1s for CP-NCNTs are shown in Figure S4b (Supporting Information). The peaks at 398.2, 399.2, and 400.7 eV are attributed to pyridinic-N, pyrrolic-N, and graphitc-N, and the peak at 404 eV is assigned to terminal N—O bonding. Following the thermal infusion process, metallic Na fills the voids of porous structure CP-NCNTs, as seen from the SEM images presented in Figure S5 (Supporting Information). Furthermore, cubic Na metal peaks are observed in the X-ray diffraction (XRD) pattern for Na@CP-NCNTs composite (Figure S6, Supporting Information), providing further confirmation for the presence of Na. XPS analysis of Na@CP-NCNTs is presented in Figure S7 (Supporting Information), in which the Na 1s and C 1s signals are present, further confirming the successful encapsulation of melted Na into the CP-NCNTs host.

To evaluate the electrochemical performance of the Na@CP-NCNTs, symmetrical coin cells (2032-type) with two identical Na@CP-NCNTs were assembled using a $NaPF_6$ contained carbonate-based electrolyte (1 M $NaPF_6$ in EC/PC). It has been demonstrated that $NaPF_6$ based carbonate-based electrolyte faces a greater number of issues compared to its

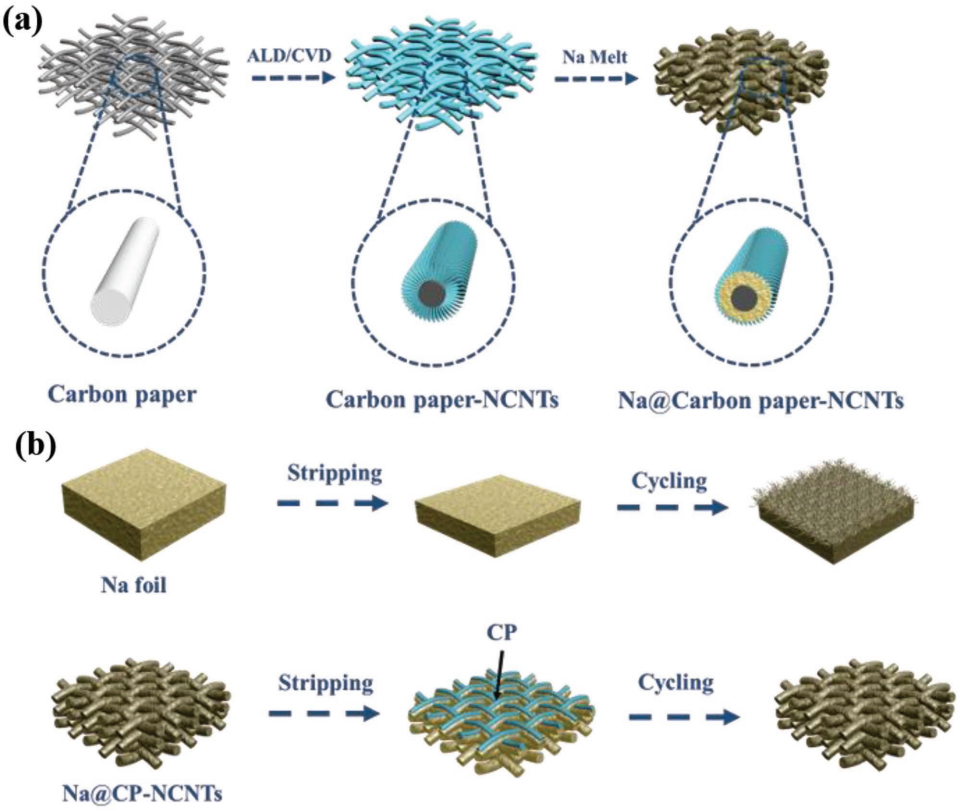

Figure 1. Schematic diagram of a) the fabrication procedure of Na@CP-NCNTs; b) the Na stripping/plating behavior occurred on the surface of Na foil and Na@CP-NCNTs.

ether-based analogue. **Figure 2**a displays the cycling stability of Na@CP-NCNTs composites and bare Na foil at a current density of 3 mA cm^{-2}. It is considered that the definition of voltage hysteresis is admitted as the mass-transfer resistant throughout the whole process. For the bare Na foil, an initial overpotential of 400 mV (vs Na^+/Na) is observed alongside a gradually increasing overpotential after 110 h of plating/stripping up to 1000 mV. For comparison, as-prepared Na@CP-NCNTs composites exhibit very stable performance, with an overpotential of only 60 mV in the first cycle and slightly increasing to 150 mV after 130 h of stripping and plating. Furthermore, the Na@CP-NCNTs composites display very stable performance and can maintain an overpotential of 200 mV after 180 h of cycling. Further increasing the current density to 5 mA cm^{-2}, the overpotential of bare Na foil begins increasing after 90 h with fluctuating voltage profiles and rising to over 1000 mV after 140 h (Figure 2b–d). The appearance of fluctuating voltage profile can be attributed to detrimental Na dendrite (moss) growth and rapid formation of dead Na, resulting in soft short circuiting. Promisingly, Na@CP-NCNTs composites can achieve stable plating/stripping performances at this elevated current density with the low overpotential of 120 mV after 140 h of cycling. Meanwhile, the long cycling performance is presented in Figure S8 (Supporting Information) at the current density of 1 mA cm^{-2} with the capacity of 1 mAh cm^{-2}. The results presented here demonstrate that the as-prepared electrodes show very stable performance up to 350 h of continuous stripping/plating with minimum changes to the voltage hysteresis. To further explore, the electrochemical performance Na@CP-NCNTs rate analysis of symmetrical cells was conducted and is presented in Figure 2e–g. The novel composite demonstrates both lower and more stable voltage polarization curves at a current density of 1, 3, 5, and 10 mA cm^{-2} compared to bare Na. The obvious difference can be attributed to high specific kinetic obstacles faced when using elevated current density. However, the Na@CP-NCNTs composites are capable of operating stably at high current density due to their high electron/ion conductivity providing ample avenues for electron/ion transport.

Herein, we demonstrate the Na@CP-NCNTs composites with a large capacity of 3 mAh cm^{-2} as compared with bare Na foil under the same testing conditions. In the presented literatures, the capacity of reported electrodes in symmetrical cell testings is always around 1 mAh cm^{-2} or even lower for both Li and Na anode, which cannot meet the requirements for practical applications and display the major advantages of large capacities (see in Table S2, Supporting Information). **Figure 3** presents cycling stability and voltage profiles of both Na@CP-NCNTs and bare Na foil using a high current density of 5 mA cm^{-2} and high capacity limit of 3 mAh cm^{-2}. The bare Na foil exhibits unstable plating/stripping behavior after 40 h of cycling with increasing overpotential increase to 2000 mV after 90 h (Figure 3). However, the Na@CP-NCNTs composites maintain a stable cycling performance with an overpotential of only 200 mV after 90 h, almost ten times lower than what was observed for bare Na foil. Based on these observations, Na@CP-NCNTs composite is an excellent candidate for use in applications that require a large capacity.

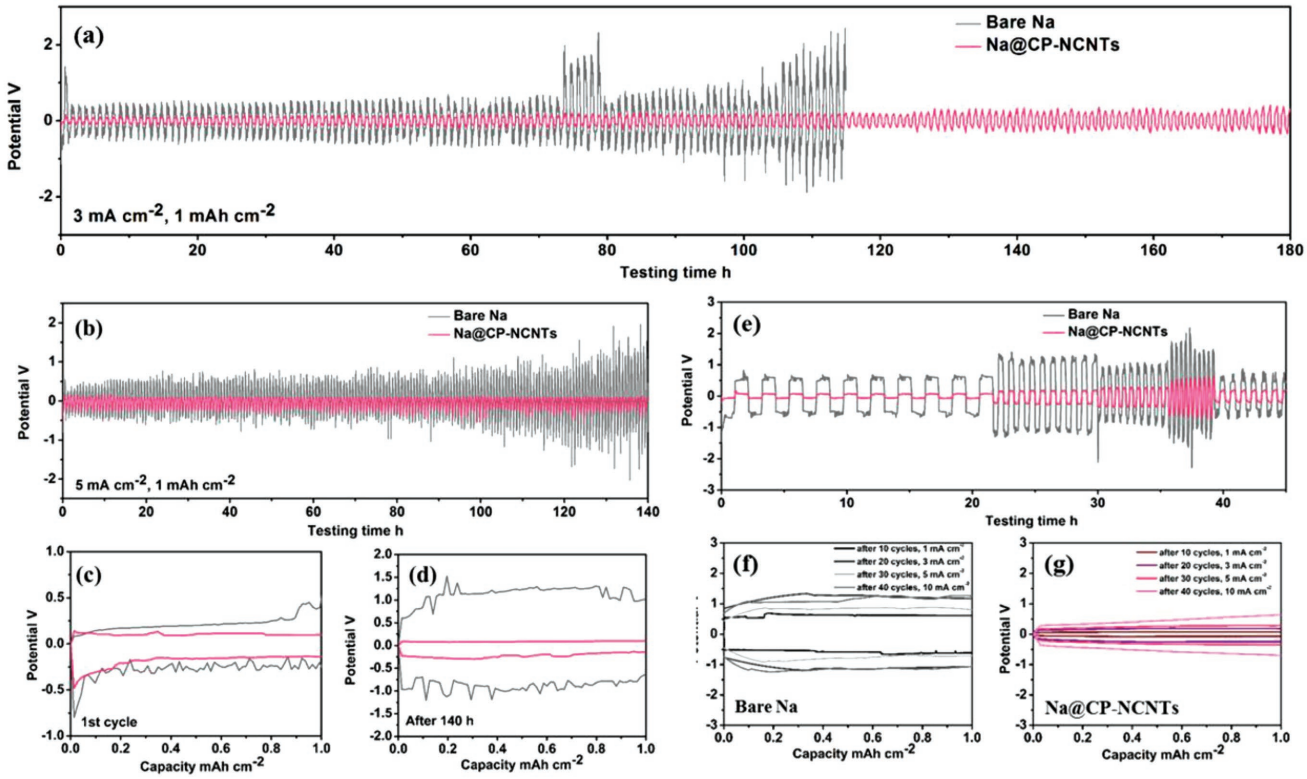

Figure 2. Comparison of the cycling stability of the Na@CP-NCNTs and the bare Na foil at a current density of a) 3 mA cm^{-2}, b) 5 mA cm^{-2} and e) the rate performances; c,d) Voltage profiles of the Na@CP-NCNTs and the bare Na foil in the different cycles at the current density of 5 mA cm^{-2}; Voltage profiles of the f) bare Na foil and the g) Na@CP-NCNTs at different stages for rate performances.

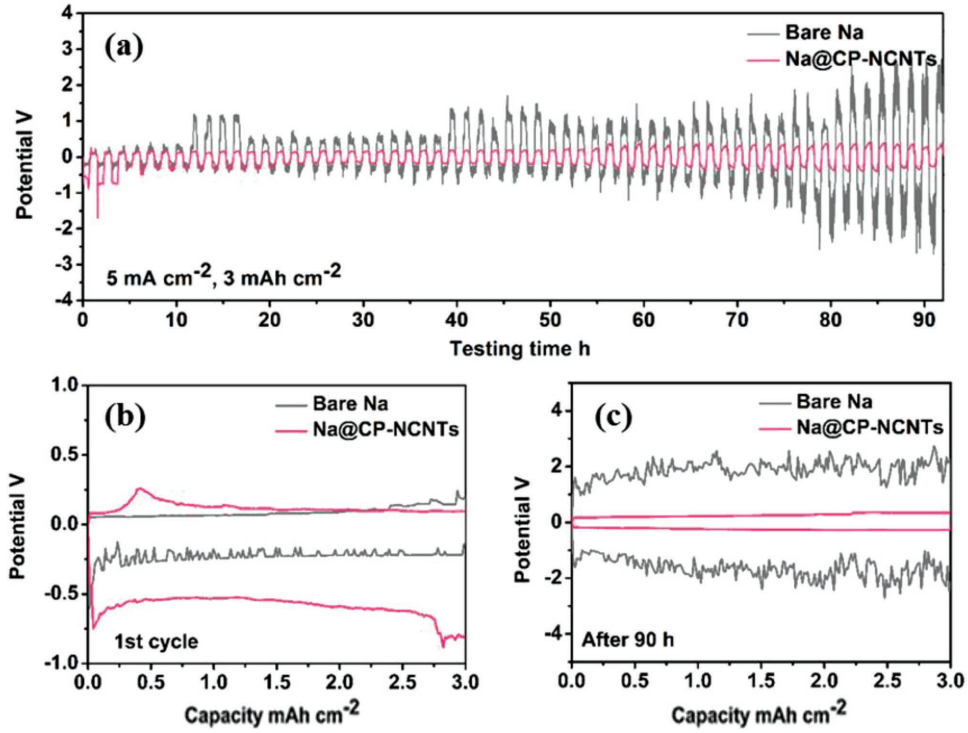

Figure 3. a) Comparison of the cycling stability of the Na@CP-NCNTs and the bare Na foil at a current density of 5 mA cm^{-2} with high capacity of 3 mAh cm^{-2}; Voltage profiles of the Na@CP-NCNTs and the bare Na foil in the b) first cycle and c) after 90 h.

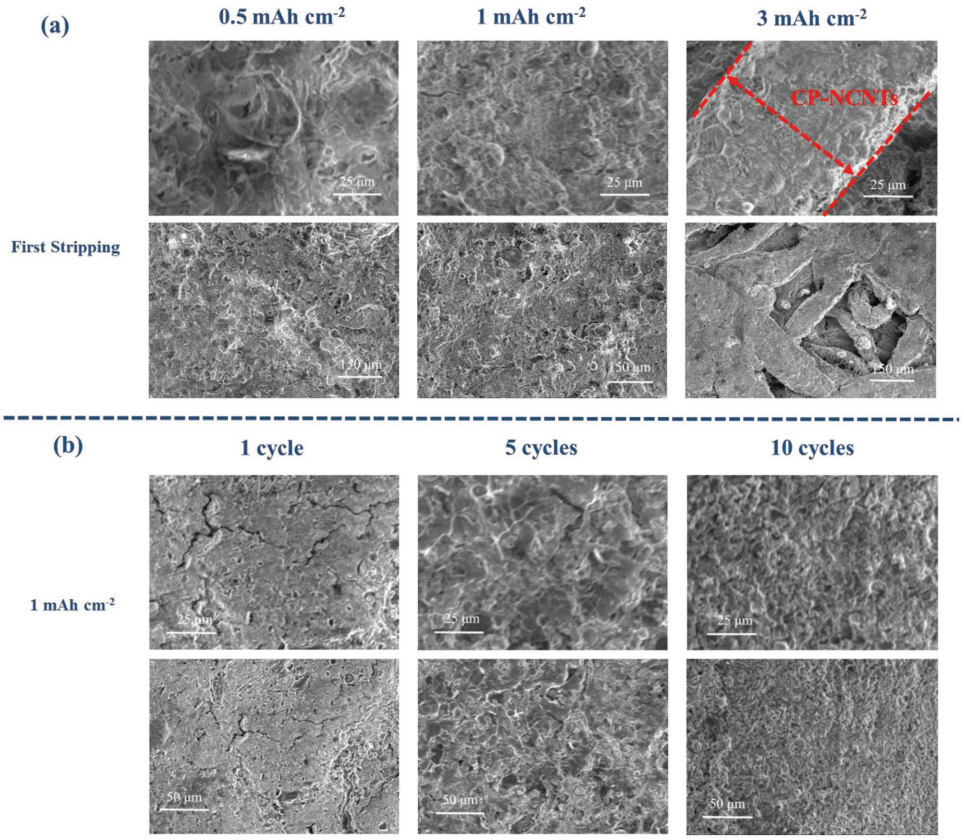

Figure 4. a) Top-view SEM images of Na@CP-NCNTs after different stripping amount of Na in the first cycle (0.5, 1, 3 mAh cm^{-2}); b) top-view SEM images of Na@CP-NCNTs after different cycles with the capacity of 1 mAh cm^{-2} (1, 5, 10 cycles).

In order to understand the effects of Na stripping and plating, morphology of our novel composite and bare Na foil was imaged following stripping of Na (0.5, 1, 3 mAh cm^{-2}) in the first cycle. Figures S9 and Figure S10 (Supporting Information) display cross-section and top-view SEM images of bare Na foil tested under the various conditions. Top-down SEM images demonstrate the appearance of large grooves following Na stripping. Furthermore, these grooves increase in size when the capacity is increased from 0.5 to 3 mAh cm^{-2}. However, the surfaces of Na@CP-NCNTs following stripping 0.5 and 1 mAh cm^{-2} is much smoother compared to bare Na, indicating uniform distribution of ions/electrons. This advantageous effect may arise from the presence of vertical NCNTs (**Figure 4**a). Interestingly, further increasing the stripping capacity to 3 mAh cm^{-2}, partial CP-NCNTs morphology can be clearly observed, indicating favorable structure retention following the high-temperature thermal infusion process and electrochemical plating/stripping. Furthermore, cross-section SEM images of the Na@CP-NCNTs following stripping (**Figure 5**a), exhibit minimum volume change, demonstrating its favorable properties.

Further, SEM measurements were conducted on bare Na foil and Na@CP-NCNTs composite after varying amounts of electrochemical cycling (1, 5, 10 cycles) using a fixed capacity of 1 mAh cm^{-2}. Figure S11 (Supporting Information) shows the images of the bare Na foil electrode (a) and Na@CP-NCNTs composites electrode (b) after 10 cycles of electrochemical plating/stripping. Our results show that the bare Na foil electrodes are covered with dark slurry which can be considered as the dropped dead Na in the electrolyte. In contrast, the Na@CP-NCNTs composites electrodes reveal the presence of pristine Na metal, indicating decreased production of dead Na. Cross-section SEM images of bare Na foil after 1, 5, and 10 cycles are shown in Figure S12 (Supporting Information). Following the first cycle, the surface of Na foil turns rough but the thickness of the foil has almost no change. However, after five electrochemical plating/stripping cycles, a thick layer of dead Na, ≈30 μm in thickness, can be seen in Figure S12b (Supporting Information). This layer is a result of detrimental side reactions occurring between Na and the organic electrolyte, leading to continuous formations of mossy-like or dendritic Na. With prolonged cycling of ten cycles, the layer of dead Na drastically increases in thickness (Figure S12c, Supporting Information), indicating large volume changes occurring for Na foil during cycling. The corresponding top-view SEM images of Na foil after 1, 5, and 10 cycles are outlined in Figure S12 (Supporting Information). With sustained electrochemical cycling, the appearance of mossy-like or dendritic Na growth becomes more obvious as the surface begins to increase in roughness, suggesting continuously side reactions and unstable SEI layer formation. Conversely, top-view SEM images (Figure 4b) of Na@CP-NCNTs electrodes after cycling, display a relatively smooth surface and lack any mossy or dendritic Na, indicating uniform Na deposition during electrochemical plating/stripping.

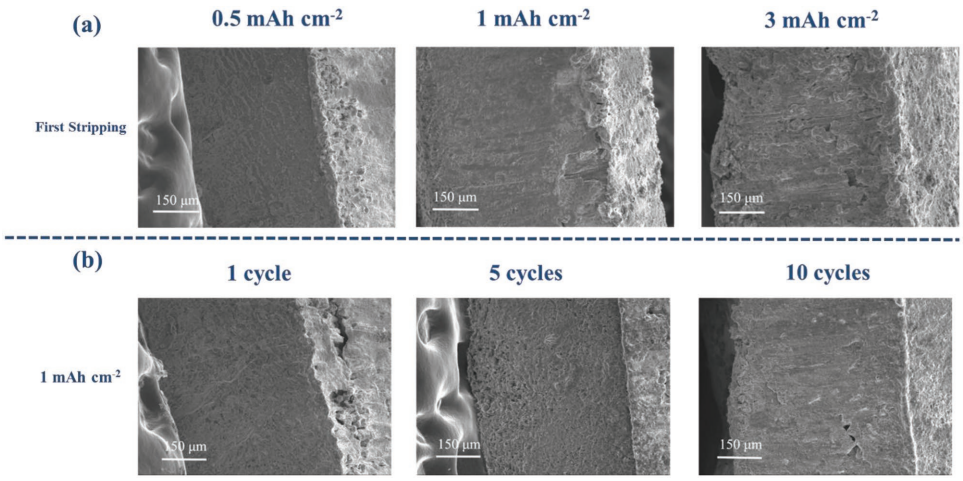

Figure 5. a) Cross section view SEM images of Na@CP-NCNTs after different stripping amount of Na in the first cycle (0.5, 1, 3 mAh cm^{-2}); b) cross section view SEM images of Na@CP-NCNTs after different cycles with the capacity of 1 mAh cm^{-2} (1, 5, 10 cycles).

Cross-section SEM images for Na@CP-NCNTs electrodes, shown in Figure 5b, exhibit a highly stable structure with negligible change in thickness. Briefly, our design of the CP-NCNTs hosted Na metal anodes demonstrate a dendrite free electrode with minimal volume change with different stripping capacities and stripping/plating cycle numbers.

To study the effect of N dopant on binding energy (BE) of Na on CNTs, we use an H-terminated nanoribbon (NR) with a width of 11.38 Å as model system. NRs are chosen so that we can also model N dopant at the edges of CNT by replacing an H–C pair with a N atom. Since we are only interested in chemisorption of Na, dispersion correction for the van der Waals interaction is not considered. Calculated BEs of Na (with respect to a bulk Na) on C atoms and N dopants at different positions, with respect to the edges as well as pyridinic and pyrrolic N sites, are listed in **Figure 6**. Our calculations show

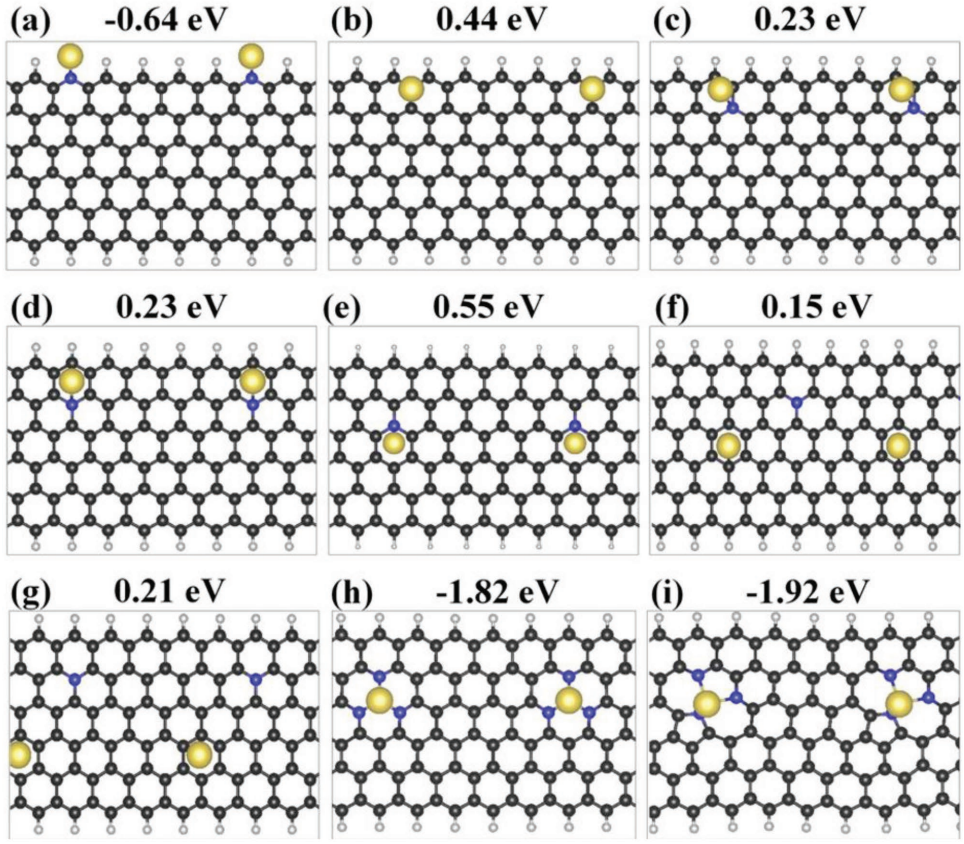

Figure 6. a–i) Atomic structures and binding energies (BE) of Na at different N-doped graphene locations.

that BEs on N dopants (Figure 6b–e) or C atoms (Figure 6f,g), which are not at the edges, are positive. However, a calculated BE of –0.64 eV for Na adsorption to N dopants at the edges of NR is strong (Figure 6a). Pyridinic (Figure 6h) and pyrrolic (Figure 6i) sites with three N atoms provide an even stronger BE of –1.82 and –1.92 eV, respectively. This represents a value which is almost three times higher than the BE of Na to one edge N dopant. This result shows a significant improvement of bond strength between Na and carbon-based materials such as CNTs by N doping.

The SEM and simulation results represent a strong consistency to the electrochemical performance obtained here in. Using this data, we present a schematic illustration in Figure 1b to represent our interpretation for the unique phenomenon observed when using this novel Na@CP-NCNTs composite electrode compared to bare Na foil. For the bare Na foil, shown in Figure 1b, the serious mossy-like and dendritic Na is produced during electrochemical plating/stripping process due to the serious side reaction with components within the electrolyte. Furthermore, rapid and prolonged formation of dead Na results in the formation of a high surface area SEI layer that consumes active Na as well as drains the cell of electrolyte. This causes the resistance of the cell to increase and diminishes cell performance. In contrast, the 3D skeleton of the CP-NCNTs electrode allows for uniform deposition of Na and lacks any surface features related to mossy or dendritic Na. During electrochemical cycling, Na is easily and uniformly removed from the skeleton structure and deposited back on the CP-NCNTs during plating. With uniform deposition occurring using a robust structure, the as-prepared Na@CP-NCNTs electrodes indicate minimum dendrite growth and volume change, resulting in excellent electrochemical performance with long life time and allows for the use of large capacity.

3. Conclusion

In conclusion, we demonstrate a unique structure of CP with NCNTs as a 3D skeleton for stable use of Na metal anode using high current density and cycling capacity. In our rational design, (1) the growth of vertical NCNTs can effectively change the Na wettability of CP from "Na-phobic" into "Na-philic"; (2) the highly conductive networks from CP and NCNTs provide homogeneous local current allowing for uniform Na stripping and plating; (3) the Na@CP-NCNTs composites show stable electrochemical plating/stripping performances under different current density, even up to 5 mA cm^{-2}. Furthermore, we also are the first to demonstrate the stable use of a high capacity of 3 mAh cm^{-2} using our unique Na@CP-NCNTs electrode. (4) The 3D skeleton structure remains intact after cycling with minimum volume change. It is believed that our design of 3D host with "Na-philic" properties opens up new opportunities to the realization of next-generation high energy density Na metal batteries.

Experimental Section

Fabrication of CP-NCNTs Composite Skeleton: ALD coatings were conducted on CP in a Gemstar-8 ALD system (Arradiance, USA). Al_2O_3 was deposited on the CP at 120 °C by using trimethylaluminium and water (H_2O) as precursors for 200 cycles. Then, the Al_2O_3-coated CP was loaded into a vertical tube furnace that was ramped from room temperature to 856 °C using an Ar flow of 200 mL min^{-1}. Catalyst ferrocene solution (solvent: acetonitrile, concentration: 0.02 g mL^{-1}) was then introduced into the quartz tube at a flow rate of 0.1 mL min^{-1} as for 5 min under Ar atmosphere. Following this, imidazole solution is injected into the quartz tube (solvent: acetonitrile, concentration: 0.2 g mL^{-1}, flow rate: 0.1 mL min^{-1}) to grow NCNT bundles for 30 min followed by cooling to room temperature. Typically, a 30 min growth yielded NCNT bundles with a length of around 20 µm.

Fabrication of Na@CP-NCNTs Composite Electrodes: As-prepared CP-NCNTs were cut into 3/8 in. disks and transferred into an Ar-filled glove box with less than 0.1 ppm water and 0.1 ppm O_2. Thermal infusion of Na melting was carried out inside the glove box. Bulk Na (from Aldrich) was cut into smaller pieces and placed in a stainless-steel boat and heated on a hot plate until Na began to melt. The prepared CP-NCNTs disk was then placed into the molten Na to obtain the Na@ CP-NCNTs composite electrodes. The weights of the CP and CP-NCNTs are 0.01 and 0.019 g, respectively. After Na thermal diffusion, the weights of Na in the composite electrodes of Na@CP-NCNTs are around 0.039–0.042 g. In this case, the theoretical specific volumetric and gravimetric capacity of the anode is 65 mAh cm^{-2} and 928 mAh g^{-1}, respectively.

Electrochemical Measurements: Electrochemical analysis was performed using CR2032 coin-type cells assembled in an ultrapure Ar-filled glove box. The cells followed a symmetrical configuration of Na/electrolyte-separator/Na with the use of polypropylene separators (Celgard 3501). The electrolyte used in this study was 1 M sodium hexafluorophosphate ($NaPF_6$ 98%, Aldrich) dissolved in ethylene carbonate (EC) and propylene carbonate (PC) with volume ratio of 1:1. Na stripping/plating studies were carried out in an Arbin BT-2000 battery test system at room temperature. Constant current densities were applied to the electrodes during repeated stripping/plating while transient potential was recorded over time.

Characterization: SEM images were taken using a Hitachi 3400N Environmental scanning electron microscopy at an acceleration voltage of 5 kV. Due to the soft properties of Na metal, Swagelok type cells comprised of Na/electrolyte-separator/Na system were used to carry out the morphology testing after stripping/plating. Swagelok cells were disassembled after ten cycles of stripping/plating in an Ar-filled glove box and gently rinsed using dimethyl carbonate to remove residual Na salts and electrolyte. SEM cross-section images of Na metal were obtained by slicing the electrode in half with the use of a sharp scissor. XPS testing was carried out using an Ar glove box connected to an XPS (Kratos AXIS Ultra Spectrometer) system. XRD testing was obtain using a Bruker D8 Advance XRD system equipped with a Cu–Kα X-ray source. Raman spectroscopy was performed using an air-sensitive holder on a HORIBA Scientific LabRAM HR system.

Theoretical Section: Density functional theory (DFT) calculations were carried out using the projector-augmented plane-wave method as implemented in the Vienna Ab Initio simulation package.[32] Perdew–Burke–Ernzerhof[33] exchange-correlation functional, a 5×5 unit cell of nanoribbon, a $2 \times 1 \times 1$ *k*-point mesh, and an energy cutoff of 450 eV were used. Vacuum spaces of ≈15 and ≈14 Å for the separation of nanoribbon edges and planes were considered to exclude image–image interaction. The convergence criteria for total energy was set at 10^{-4} eV.

Supporting Information

Supporting Information is available from the Wiley Online Library or from the author.

Acknowledgements

Y.Z. and X.Y. contributed equally to this work. X.S. conceived the overall project. Y.Z., X.Y., and X.S. designed/performed the experiments. Y.Z.

completed the data analysis and wrote the manuscript. L.K. and P.K. carried out the DFT calculations. Q.S., J.L., and B.W. performed the physical characterizations. A.L., R.L., and H.Z. interpreted the results and data analysis. All authors read and commented on the manuscript. This research was supported by the Natural Science and Engineering Research Council of Canada (NSERC), the Canada Research Chair Program (CRC), the Canada Foundation for Innovation (CFI), and the University of Western Ontario (UWO). P.K. gratefully acknowledges support from the "Bundesministerium für Bildung und Forschung" (BMBF) as well as the Gauss Centre for Supercomputing e.V. (www.gauss-centre.eu) for funding this project and providing computing time on the GCS Supercomputer SuperMUC at Leibniz Supercomputing Centre (www.lrz.de).

Conflict of Interest

The authors declare no conflict of interest.

Keywords

3D Na anodes, metallic sodium anodes, Na-philic, sodium metal batteries

Received: October 25, 2017
Revised: January 23, 2018
Published online: April 15, 2018

[1] Y. Zhao, X. F. Li, B. Yan, D. B. Xiong, D. J. Li, S. Lawes, X. L. Sun, *Adv. Energy Mater.* **2016**, *6*, 1502175.
[2] Y. Zhao, Z. Song, X. Li, Q. Sun, N. Cheng, S. Lawes, X. Sun, *Energy Storage Mater.* **2016**, *2*, 35.
[3] Y. Zhao, X. Li, B. Yan, D. Li, S. Lawes, X. Sun, *J. Power Sources* **2015**, *274*, 869.
[4] J. Lang, L. Qi, Y. Luo, H. Wu, *Energy Storage Mater.* **2017**, *7*, 115.
[5] S. Wei, S. Choudhury, J. Xu, P. Nath, Z. Tu, L. A. Archer, *Adv. Mater.* **2017**, *29*, 1605512.
[6] Y. J. Kim, H. Lee, H. Noh, J. Lee, S. Kim, M. H. Ryou, Y. M. Lee, H. T. Kim, *ACS Appl. Mater. Interfaces* **2017**, *9*, 6000.
[7] H. Yadegari, M. Norouzi Banis, A. Lushington, Q. Sun, R. Li, T.-K. Sham, X. Sun, *Energy Environ. Sci.* **2017**, *10*, 286.
[8] Z. E. Reeve, C. J. Franko, K. J. Harris, H. Yadegari, X. Sun, G. R. Goward, *J. Am. Chem. Soc.* **2017**, *139*, 595.
[9] C. Xia, R. Fernandes, F. H. Cho, N. Sudhakar, B. Buonacorsi, S. Walker, M. Xu, J. Baugh, L. F. Nazar, *J. Am. Chem. Soc.* **2016**, *138*, 11219.
[10] W.-J. Kwak, Z. Chen, C. S. Yoon, J.-K. Lee, K. Amine, Y.-K. Sun, *Nano Energy* **2015**, *12*, 123.
[11] Q. Sun, H. Yadegari, M. N. Banis, J. Liu, B. Xiao, X. Li, C. Langford, R. Li, X. Sun, *J. Phys. Chem. C* **2015**, *119*, 13433.
[12] H. Yadegari, M. N. Banis, B. Xiao, Q. Sun, X. Li, A. Lushington, B. Wang, R. Li, T.-K. Sham, X. Cui, X. Sun, *Chem. Mater.* **2015**, *27*, 3040.
[13] H. Yadegari, Y. Li, M. N. Banis, X. Li, B. Wang, Q. Sun, R. Li, T.-K. Sham, X. Cui, X. Sun, *Energy Environ. Sci.* **2014**, *7*, 3747.
[14] T. T. Zuo, X. W. Wu, C. P. Yang, Y. X. Yin, H. Ye, N. W. Li, Y. G. Guo, *Adv. Mater.* **2017**, *29*, 1700389.
[15] Y. Guo, H. Li, T. Zhai, *Adv. Mater.* **2017**, *29*, 1700007.
[16] D. Lin, Y. Liu, Y. Cui, *Nat. Nanotechnol.* **2017**, *12*, 194.
[17] R. Pinedo, D. A. Weber, B. Bergner, D. Schröder, P. Adelhelm, J. Janek, *J. Phys. Chem. C* **2016**, *120*, 8472.
[18] L. Lutz, W. Yin, A. Grimaud, D. Alves Dalla Corte, M. Tang, L. Johnson, E. Azaceta, V. Sarou-Kanian, A. J. Naylor, S. Hamad, J. A. Anta, E. Salager, R. Tena-Zaera, P. G. Bruce, J. M. Tarascon, *J. Phys. Chem. C* **2016**, *120*, 20068.
[19] W. Luo, Y. Zhang, S. Xu, J. Dai, E. Hitz, Y. Li, C. Yang, C. Chen, B. Liu, L. Hu, *Nano Lett.* **2017**, *17*, 3792.
[20] Y. Zhao, L. V. Goncharova, A. Lushington, Q. Sun, H. Yadegari, B. Wang, W. Xiao, R. Li, X. Sun, *Adv. Mater.29*, **2017**, 1606663.
[21] Z. W. Seh, J. Sun, Y. Sun, Y. Cui, *ACS Cent. Sci.* **2015**, *1*, 449.
[22] X. Meng, X. Q. Yang, X. Sun, *Adv. Mater.* **2012**, *24*, 3589.
[23] X. Meng, *Nanotechnology* **2015**, *26*, 020501.
[24] W. Luo, C.-F. Lin, O. Zhao, M. Noked, Y. Zhang, G. W. Rubloff, L. Hu, *Adv. Energy Mater.* **2017**, *7*, 1601526.
[25] Y. Zhao, L. V. Goncharova, Q. Zhang, P. Kaghazchi, Q. Sun, A. Lushington, B. Wang, R. Li, X. Sun, *Nano Lett.* **2017**, *17*, 5653.
[26] D. Lin, Y. Liu, Z. Liang, H. W. Lee, J. Sun, H. Wang, K. Yan, J. Xie, Y. Cui, *Nat. Nanotechno l.* **2016**, *11*, 626.
[27] Y. Liu, D. Lin, Z. Liang, J. Zhao, K. Yan, Y. Cui, *Nat. Commun.* **2016**, *7*, 10992.
[28] Z. Liang, D. Lin, J. Zhao, Z. Lu, Y. Liu, C. Liu, Y. Lu, H. Wang, K. Yan, X. Tao, Y. Cui, *Proc. Natl. Acad. Sci. USA* **2016**, *113*, 2862.
[29] R. Zhang, X. Chen, X. Cheng, X. Zhang, C. Yan, Q. Zhang, *Angew. Chem., Int. Ed.* **2017**, *56*, 7764.
[30] X. Hu, Z. Li, Y. Zhao, J. Sun, Q. Zhao, J. Wang, Z. Tao, J. Chen, *Sci. Adv.* **2017**, *3*, e1602396.
[31] J. Chen, J. Z. Wang, A. I. Minett, Y. Liu, C. Lynam, H. Liu, G. G. Wallace, *Energy Environ. Sci.* **2009**, *2*, 393.
[32] G. Kresse, J. Furthmüller, *Phys. Rev. B* **1996**, *54*, 11169.
[33] J. Perdew, K. Burke, M. Ernzerhof, *Phys. Rev. Lett.* **1996**, *77*, 3865.